Electronic Supplementary Material (ESI) for Journal of Materials Chemistry C.

Supplementary Information for manuscript: "Realization of the electrical-field driven "one-material"-based magnetic tunnel junction using van der Waals antiferromagnetic $MnPX_3$ (X: S, Se)"

Jin Yichen,[1] Mouhui Yan,[1] Yuriy Dedkov,[1,2,a] Elena Voloshina,[1,2,3,b]

[1]*Department of Physics, Shanghai University,*

99 Shangda Road, 200444 Shanghai, P. R. China

[2]*Centre of Excellence ENSEMBLE3 Sp. z o. o.,*

Wolczynska Str. 133, 01-919 Warsaw, Poland and

[3]*Institute of Chemistry and Biochemistry,*

Freie Universität Berlin, Arnimallee 22, Berlin, Germany

[a] Corresponding author. E-mail: yuriy.dedkov@icloud.com

[b] Corresponding author. E-mail: elena.voloshina@icloud.com

List of Supplementary Material:

- Structure, electronic and magnetic properties of bulk $MnPX_3$
- Electronic and magnetic state of the $MnPX_3$ monolayers
- Electronic and magnetic structure of the Li:2D-$MnPX_3$ and F:2D-$MnPX_3$ systems
- Tab. S1: Results obtained for the different magnetic states of 3D-$MnPX_3$ with PBE+U+D2: ΔE (in eV) is the difference between the total energy calculated for the given symmetry/magnetic states and the total energy calculated for the ground state, a, c (in Å) are the optimised lattice parameters, d_0 (in Å) is the van der Waals gap of bulk crystal.
- Tab. S2: Results obtained for the different magnetic states of 2D-$MnPS_3$ and 2D-$MnPSe_3$ with PBE+U+D2: E (in eV per (2×2) unit cell) is the total energy; ΔE (in meV) is the difference between the total energy calculated for the magnetic states and the total energy calculated for the nAFM state. Band gap (E_g, in eV), Mn^{2+} magnetic moment (M, in μ_B), the exchange coupling parameters between two local spins (J, in meV), and Néel temperature (T_{N}, in K) are given for the lowest-energy structure.
- Tab. S3: Relative to the lowest energy values (in eV per (2×2) unit cell) for the different magnetic states of 2D-$MnPS_3$ and 2D-$MnPSe_3$ upon adsorption of Li, Cl, and F as obtained with PBE+U+D2. For the notation used to indicate different adsorption sites, see Figure S1.
- Tab. S4: Results obtained with PBE $+U$ + D2 for the ground states of 2D-$MnPS_3$ and 2D-$MnPSe_3$ upon adsorption of Li, Cl, and F in the concentration of 1/4 ML for their most stable adsorption configuration: ΔE_{ads} (in eV) is adsorption energy; J_1, J_2, J_3 (in meV) are the exchange coupling parameters between two local spins; T (in K) is a critical temperature; MAE (in meV per u.c.) is magnetic anisotropy energy.
- Tab. S5: Results obtained with PBE $+U$ + D2 for the ground states of 3D-$MnPS_3$ and 3D-$MnPSe_3$ upon adsorption of Li and F in the concentration of 1/4 ML for their most stable adsorption configuration: ΔE_{ads} (in eV) is adsorption energy; J_1, J_2, J_3 (in meV) are the exchange coupling parameters between two local spins; T (in K) is a

critical temperature; E_g (in eV) is band gap (two values for the spin-up and spin-down channels are indicated).

- Fig. S1: *ABC*-sequence of layers in 3D $MnPX_3$. For simplicity, only Mn-ions are shown. Atoms of different layers are shown with spheres of different size and style. In (a) the in-plane and out- of-plane lattice constants are indicated with letters a and c, respectively; (b) and (c) highlight the difference between stackings in $MnPS_3$ and $MnPSe_3$.

- Fig. S2: Top (a) and side (b) views of a single layer of MPX_3. Spheres of different size/colour represent ions of different type. The adsorption sites considered in this work are marked with different symbols.

- Fig. S3: Band structures and site-projected density of states for (a) 3D-$MnPS_3$, (b) 3D-$MnPSe_3$.

- Fig. S4: Spin-resolved band structures and site-projected density of states for (a) 2D-$MnPS_3$, (b) Li:2D-$MnPS_3$, (c) Cl:2D-$MnPS_3$ (d) F:2D-$MnPS_3$.

- Fig. S5: Spin-resolved band structures and site-projected density of states for (a) 2D-$MnPSe_3$, (b) Li:2D-$MnPSe_3$, (c) Cl:2D-$MnPSe_3$ (d) F:2D-$MnPSe_3$.

- Fig. S6: Specific heat capacity per spin with respect to temperature for (a) 2D-$MnPX_3$, (b) Li:2D-$MnPX_3$, (c) Cl:2D-$MnPX_3$, (d) F:2D-$MnPX_3$.

- Fig. S7: Top and side views of the studied systems in their lowest energy configurations. Spheres of different size and colour represent atoms of different types (cf. Figure S1). The structures are overlaid with an electron charge difference maps $\Delta\rho(\mathbf{r}) = \rho_{\mathrm{sub/ads}}(\mathbf{r}) - [\rho_{\mathrm{sub}}(\mathbf{r}) + \rho_{\mathrm{ads}}(\mathbf{r})]$ (sub: substrate, ads: adsorbate). $\Delta\rho$ is colour coded as blue ($-0.01\,e/\mathrm{\AA}^3$), green (0), and red ($0.01\,e/\mathrm{\AA}^3$).

- Fig. S8: Specific heat capacity per spin with respect to temperature for (a) Li:3D-$MnPS_3$, (b) F:3D-$MnPS_3$, (c) Li:3D-$MnPSe_3$, (d) F:3D-$MnPSe_3$.

Structure, electronic and magnetic properties of bulk $MnPX_3$

3D bulk MPX_3 crystals usually adopt either $C2/m$ or $R\bar{3}$ space group. Both of them can be represented in hexagonal unit cells. Then every unit cell contains three MPX_3 single layers having D_{3d} symmetry (Figure S1), which are stacked in a different way (Figure S2). Each single-layer are held together by van der Waals forces. The lattice parameters of hexagonal 3D $MnPX_3$ were fully relaxed in nonmagnetic (NM), ferromagnetic (FM) and Néel antiferromagnetic (nAFM) states and they are listed in Table S1 with the respective relative energies. Thus, bulk $MnPS_3$ crystallizes in the $C2/m$ space group, while $MnPSe_3$ in $R\bar{3}$ and both of them adopt the AFM ground state (Table S1), that is in agreement with available experimental and theoretical data [1–3]. The band structure and density of states (DOS) calculated for the ground-state structures of 3D $MnPS_3$ and $MnPSe_3$ are shown in Figure S3. From these results one can see, that the both systems under study are indirect band gaps semiconductors. The bands in the vicinity of the Fermi energy are mostly composed of S/Se p-orbitals with a significant contribution form the Mn d orbitals.

Electronic and magnetic state of the $MnPX_3$ monolayers

Our calculations show that 2D-$MnPX_3$ crystals prefer the AFM coupling of magnetic moments in their ground state (Table S2). The high-spin configuration of Mn^{2+} results in $M_{Mn} = 4.6\,\mu_B$. In agreement with the previous studies [3], the calculated electronic band structure indicates that the both 2D $MnPX_3$ crystals are wide band-gap semiconductors with an indirect band gaps of 2.50 eV and 1.84 eV, respectively (Figure S4a and Figure S5a). The band structures are spin-degenerated in the AFM state, showing similar features for both studied materials. The bands in the vicinity of the Fermi energy are mostly composed of S/Se p-orbitals with a significant contribution form the Mn d orbitals (Figure S4a and Figure S5a). The calculated magnetic exchange coupling parameters are $J_1 = -0.65$ meV, $J_2 = -0.03$ meV, $J_3 = -0.21$ meV, for $MnPS_3$, and $J_1 = -0.40$ meV, $J_2 = -0.03$ meV, $J_3 = -0.19$ meV, for $MnPSe_3$, confirm that both monolayers under study are in a robust Néel AFM (nAFM) phase. The above J-values are used in simulations of Néel temperatures (T_N) which result in 87 K and 61 K, for for $MnPS_3$ and $MnPSe_3$ (Figure S6a), respectively.

Electronic and magnetic structure of the Li:2D-$MnPX_3$ and F:2D-$MnPX_3$ systems

Upon deposition above $MnPX_3$ (X: S; Se) (Figure S1), Li-atom occupies the Mn adsorption site (Table S3) with the distances between Li-atom and the three neighbouring X-ions of 2.43 Å and 2.55 Å for X = S and Se, respectively. The relaxed structures superimposed with the charge density differences are presented in Figure S7a,d. One can note significant charge transfer from the adsorbate to the substrate and its accumulation between Li and the neighbouring X-ions. For the both X = S/Se, adsorption of Li yields stabilisation of the FM state (Tables S3 and S4). The DOS plots calculated for the ground-state structures of 1/4 ML-Li:2D-$MnPX_3$ are shown in Figure S4b and Figure S5b. The n-doping due to the Li adsorption yields a transition of $MnPX_3$ into metallic states and both systems under consideration show the HFM behaviour with the insulating spin-up channel (E_g = 2.27 eV and 1.34 eV, respectively) and metallic spin-down one. The orbitals of Mn, P, and S(Se) contribute to the states in the vicinity of E_F with almost equal weight.

Using the calculated exchange parameters, which are positive in accordance with the FM ground state, we have employed the Monte Carlo simulations based on the Ising model in order to evaluate the Curie temperatures (Figure S6). The calculated T_C, listed in Table S4, can be raised when increasing the concentration of the adsorbate. The test calculations performed using only J_1 allows us to estimate the increase of T_C by up to 40 % when enlarging the Li concentration till 1/3 ML.

When considering the halogen adsorption, both F and Cl atoms tend to stay above $[P_2X_6]^{4-}$. At that, while F is coordinated directly above P ($d(F-P)$ = 1.61 Å and 1.67 Å, for $MnPS_3$ and $MnPSe_3$, respectively), the adsorbed Cl occupies the Bridge-1 position ($d(Cl-S)$ = 2.53 Å and $d(Cl-Se)$ = 2.62 Å) (Table S3). This deviation can be attributed to the difference in atomic size of the employed halogen.

The adsorption of Cl do not tend to change the magnetic state of the substrate, and for the both X = S and Se the system prefer to stay in the AFM ground state (Table S3). The relaxed structures superimposed with the charge density differences are presented in Figure S7 b,e. One can clearly see the charge transfer from substrate to the adsorbate. This effect is also reflected in the calculated DOS (Figure S4c and S5c). Besides overall upward shift, adsorption of Cl above $MnPX_3$ (X: S, Se) results in the formation of two strongly localised states - an occupied one in the spin-up channel and an empty one in the spin-down

channel. Both states have predominantly S/Se-p character with somewhat contribution from the Mn-3d states. This leads to reduction of a band gap for spin-down states to 1.13 eV and 0.86 eV for $MnPS_3$ and $MnPSe_3$, respectively. The band gap fo spin-up states remains almost unchanged: $E_g = 2.31$ eV and 1.78 eV, for $MnPS_3$ and $MnPSe_3$, respectively. The calculated magnetic exchange coupling parameters as well as Néel temperatures (T_N) are listed in Table S4 (Figure S6c).

In the case of F the interaction between $MnPX_3$ and the adsorbate is so strong that the structure of substrate is significantly changed (Figure S7c,f). While adsorption of F above $MnPS_3$ have qualitatively similar effect as compared to the adsorption of Cl (Table S4, Figure S4d, Figure S7c), utilisation of $MnPSe_3$ as a substrate results in a more attractive picture. In the latter case, p-doping (Figure S7e) yields stabilisation of an FM state with $T_C = 96$ K (Table S4, Figure S6d). Similarly to Li:2D-$MnPX_3$, one observes the HFM behaviour, yet in the case of F-adsorption with the metallic spin-up channel and insulating spin-down one with $E_g = 1.95$ eV (Figure S5d). Thus, the spin polarisation direction of $MnPSe_3$ can be manipulated by changing the adsorbate nature. It is interesting to note, that the transition from AFM to the FM state can be achieved also for $MnPS_3$ when increasing the concentration of F up to 1/3 ML. Still, it does not show the HMF behaviour.

---

[1] Ouvrard, G., Brec, R., & Rouxel, J. Structural determination of some MPS_3 layered phases (M = Mn, Fe, Co, Ni and Cd). *Mater. Res. Bull.* **20**, 1181 – 1189 (1985).

[2] Wiedenmann, A., Rossat-Mignod, J., Louisy, A., Brec, R. & Rouxe, J. Neutron diffraction study of the layered compounds $MnPSe_3$ and $FePSe_3$. *Solid State Commun.* **40**, 1067 – 1072 (1981).

[3] Yang, J., Zhou, Y., Guo, Q., Dedkov, Y. & Voloshina, E. Electronic, magnetic and optical properties of $MnPX_3$ (X = S, Se) monolayers with and without chalcogen defects: A first-principles study, *RSC Adv.* **10**, 851 (2020).

TABLE S1. Results obtained for the different magnetic states of 3D-$MnPX_3$ with PBE+U+D2: ΔE (in eV) is the difference between the total energy calculated for the given symmetry/magnetic states and the total energy calculated for the ground state, a, c (in Å) are the optimised lattice parameters, d_0 (in Å) is the van der Waals gap of bulk crystal.

X	Symmetry	Magn. state	ΔE	a	c	d_0
S	$C/2m$	NM	26.198	5.764	19.182	3.301
		FM	0.163	6.085	19.774	3.284
		AFM	0	6.075	19.772	3.282
	$R\bar{3}$	NM	26.213	5.765	19.112	3.280
		FM	0.171	6.085	19.674	3.247
		AFM	0.011	6.076	19.683	3.249
Se	$C/2m$	NM	26.573	6.103	19.776	3.351
		FM	0.108	6.410	20.088	3.283
		AFM	0.047	6.399	20.329	3.284
	$R\bar{3}$	NM	26.528	6.109	19.541	3.276
		FM	0.162	6.408	20.300	3.210
		AFM	0	6.402	20.137	3.226

TABLE S2. Results obtained for the different magnetic states of 2D-$MnPS_3$ and $MnPSe_3$ with PBE+U+D2: E (in eV per (2×2) unit cell) is the total energy; ΔE (in meV) is the difference between the total energy calculated for the magnetic states and the total energy calculated for the nAFM state. Band gap (E_g, in eV), Mn^{2+} magnetic moment (M, in μ_B), the exchange coupling parameters between two local spins (J, in meV), and Néel temperature (T_{N}, in K) are given for the lowest-energy structure.

X	Magn. state	E	ΔE	E_g	M	J_1	J_2	J_3	T_{N}
S	FM	−224.635	219						
	nAFM	−224.854	0	2.50	4.6	−0.65	−0.03	−0.21	87
	zAFM	−224.755	99						
	sAFM	−224.757	97						
Se	FM	−205.477	151						
	nAFM	−205.628	0	1.84	4.6	−0.40	−0.03	−0.19	61
	zAFM	−205.569	58						
	sAFM	−205.554	74						

TABLE S3. Relative to the lowest energy values (in eV per (2×2) unit cell) for the different magnetic states of 2D-$MnPS_3$ and 2D-$MnPSe_3$ upon adsorption of Li, Cl, and F as obtained with PBE+U+D2. For the notation used to indicate different adsorption sites, see Figure S1.

Substrate	Adsorbate	Magn. state	Adsorption site					
			X-1	X-2	Mn	P	Bridge-1	Bridge-2
$MnPS_3$	Li	nAFM	1.0374	0.1807	0.2251	0.7526	0.6492	0.6737
		FM	0.8097	0.1009	0	0.5071	0.5367	0.5887
	Cl	nAFM	0.0546	0.2795	0.3706	0.3197	0	0.1195
		FM	0.1964	0.4596	0.5220	0.2375	0.1713	0.2880
	F	nAFM	1.1818	1.3963	1.7065	0	1.0583	1.1472
		FM	1.2924	1.5359	1.7948	0.1544	1.2175	1.2175
$MnPSe_3$	Li	nAFM	0.9299	0.0972	0.0916	0.5032	0.6873	0.5982
		FM	0.8195	0.0524	0	0.3193	0.5653	0.5867
	Cl	nAFM	0.1196	0.2428	0.4008	0.2002	0	0.1157
		FM	0.1820	0.3305	0.4378	0.0581	0.1067	0.1975
	F	nAFM	1.1583	1.1363	1.4515	0.1668	0.9067	0.9903
		FM	1.2011	1.1139	1.4270	0	0.9950	0.9951

TABLE S4. Results obtained with PBE $+U$ + D2 for the ground states of 2D-$MnPS_3$ and 2D-$MnPSe_3$ upon adsorption of Li, Cl, and F in the concentration of 1/4 ML for their most stable adsorption configuration: ΔE_{ads} (in eV) is adsorption energy; J_1, J_2, J_3 (in meV) are the exchange coupling parameters between two local spins; T (in K) is a critical temperature; MAE (in μeV per u.c.) is the out-of-plane magnetic anisotropy energy.

Substrate	Adsorbate	Magn. state	J_1	J_2	J_3	T	MAE
$MnPS_3$	Li	FM	0.81	0.34	0.09	191	6.93
	Cl	nAFM	−0.55	0.02	−0.10	84	0.20
	F	nAFM	−0.53	0.03	−0.07	76	0.15
$MnPSe_3$	Li	FM	0.42	0.24	0.02	113	36.72
	Cl	nAFM	−0.25	−0.03	−0.18	44	1.10
	F	FM	0.06	0.05	0.61	96	4.75

TABLE S5. Results obtained with PBE $+U$ + D2 for the ground states of 3D-$MnPS_3$ and 3D-$MnPSe_3$ upon adsorption of Li and F in the concentration of 1/4 ML for their most stable adsorption configuration: ΔE_{ads} (in eV) is adsorption energy; J_1, J_2, J_3 (in meV) are the exchange coupling parameters between two local spins; T (in K) is a critical temperature; E_g (in eV) is band gap (two values for the spin-up and spin-down channels are indicated).

Substrate	Adsorbate	Magn. state	J_1	J_2	J_3	T	E_g
3D-$MnPS_3$	Li	FM	0.79	0.36	0.08	198	1.89/0
	F	nAFM	−0.53	0.03	−0.13	82	0.79/2.09
3D-$MnPSe_3$	Li	FM	0.44	0.26	0.04	126	1.35/0
	F	FM	−0.01	0.08	0.52	85	0/1.36

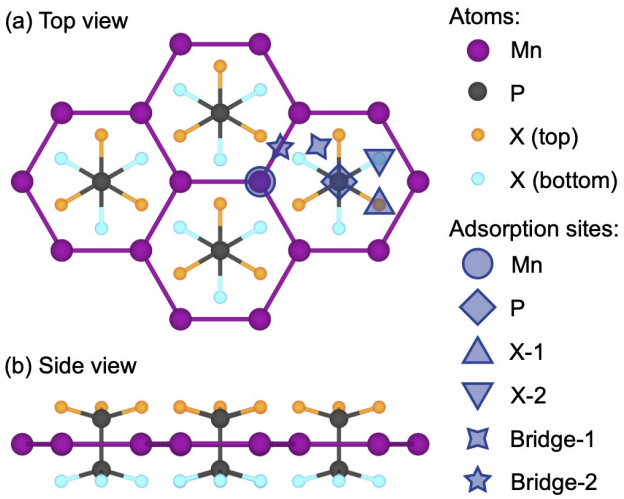

FIG. S1. Top (a) and side (b) views of a single layer of MPX_3. Spheres of different size/colour represent ions of different type. The adsorption sites considered in this work are marked with different symbols.

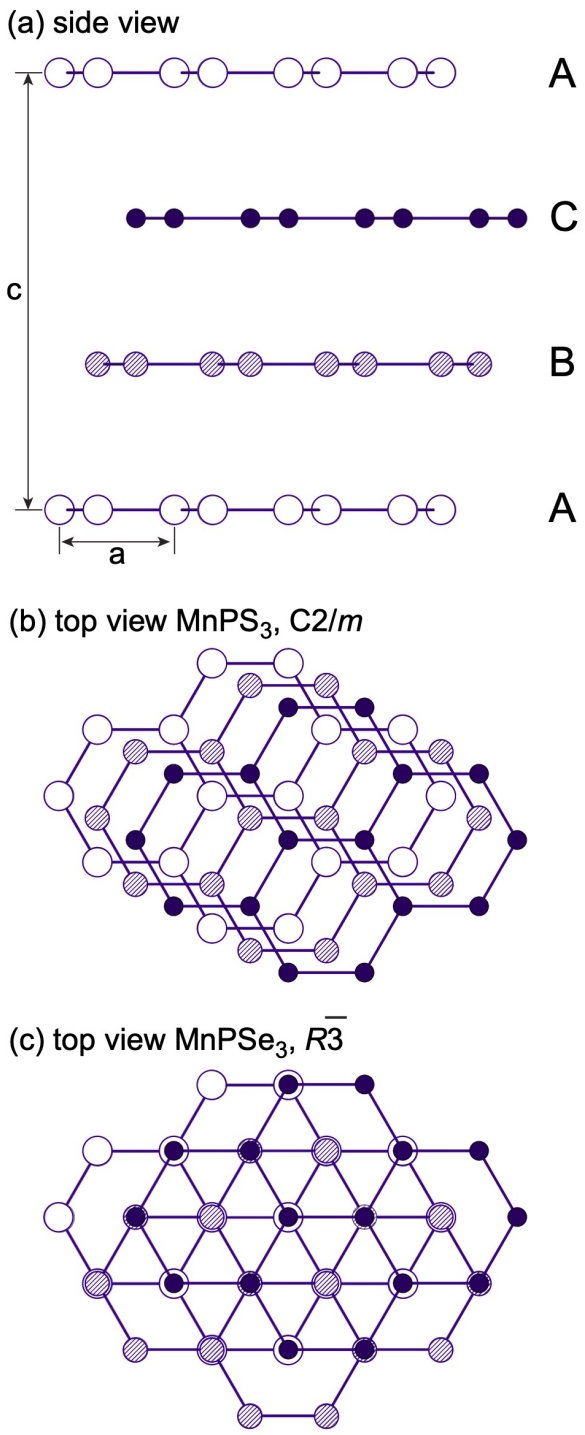

FIG. S2. *ABC*-sequence of layers in 3D $MnPX_3$. For simplicity, only Mn-ions are shown. Atoms of different layers are shown with spheres of different size and style. In (a) the in-plane and out-of-plane lattice constants are indicated with letters a and c, respectively; (b) and (c) highlight the difference between stackings in $MnPS_3$ and $MnPSe_3$.

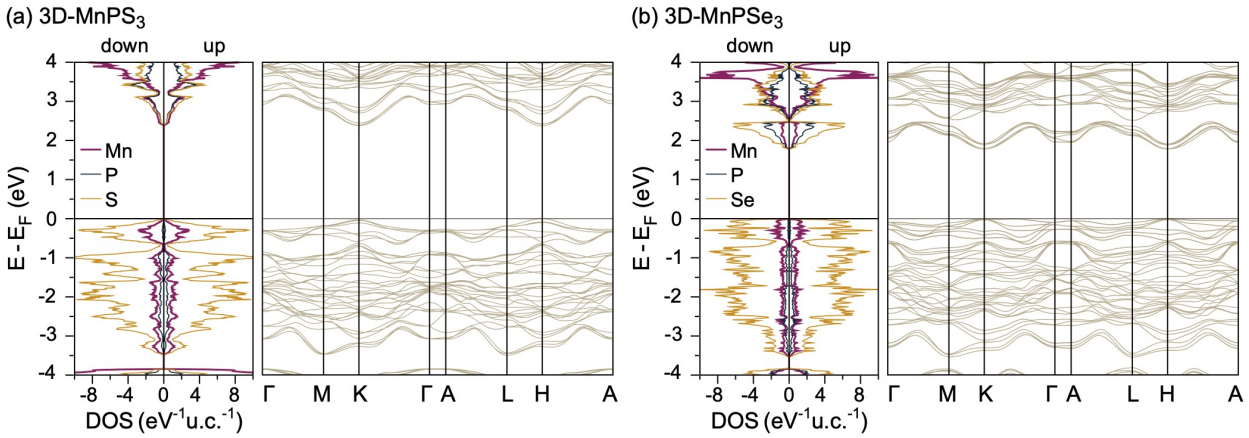

FIG. S3. Band structures and site-projected density of states for (a) 3D-$MnPS_3$, (b) 3D-$MnPSe_3$.

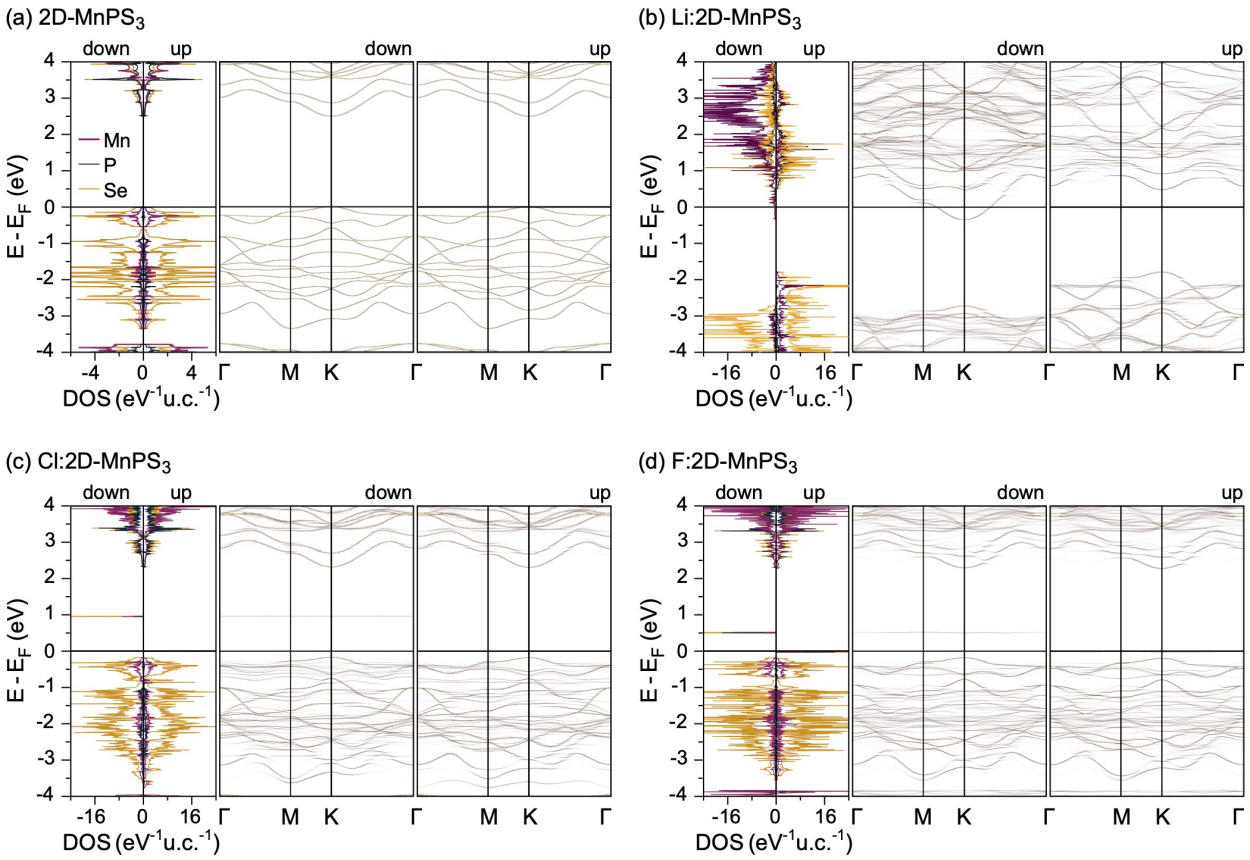

FIG. S4. Spin-resolved band structures and site-projected density of states for (a) 2D-$MnPS_3$, (b) Li:2D-$MnPS_3$, (c) Cl:2D-$MnPS_3$ (d) F:2D-$MnPS_3$.

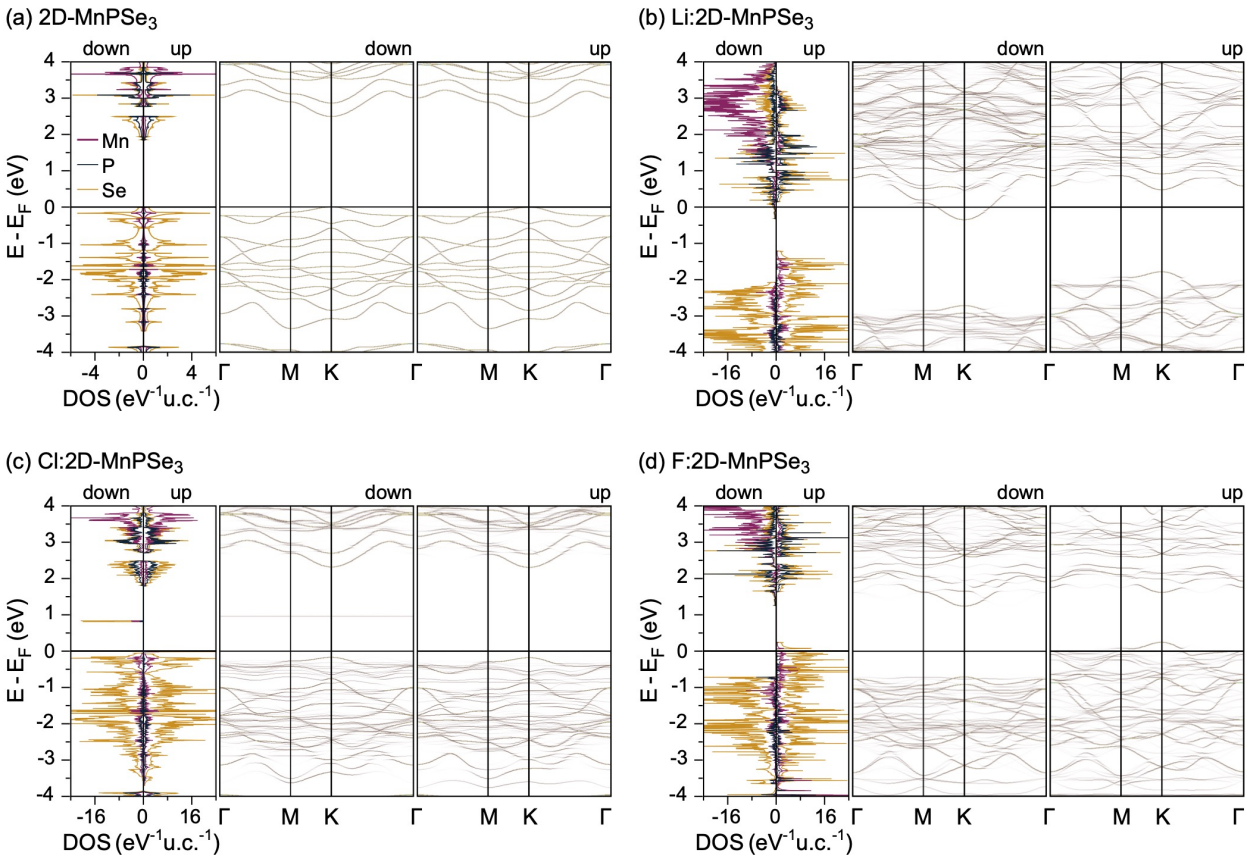

FIG. S5. Spin-resolved band structures and site-projected density of states for (a) 2D-$MnPSe_3$, (b) Li:2D-$MnPSe_3$, (c) Cl:2D-$MnPSe_3$ (d) F:2D-$MnPSe_3$.

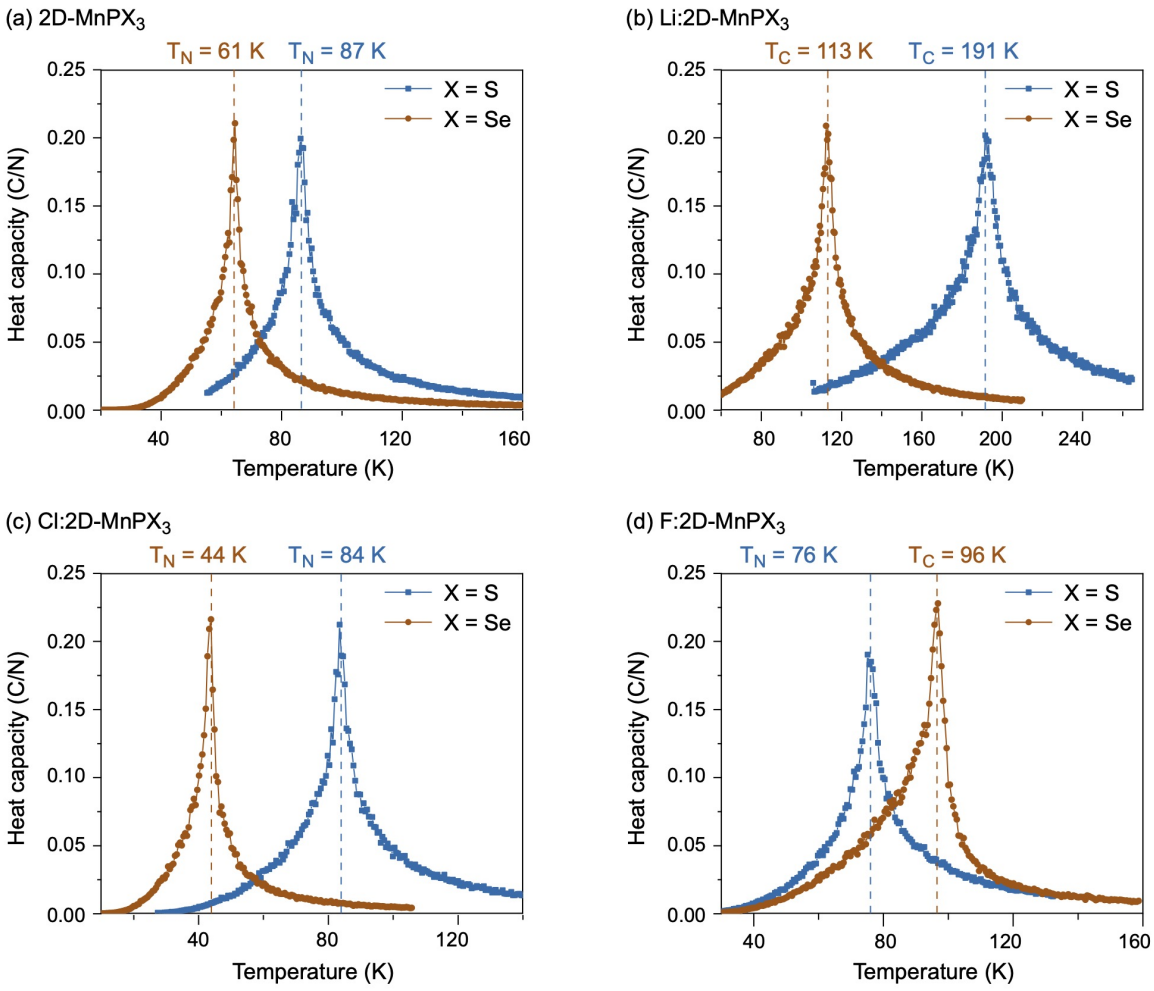

FIG. S6. Specific heat capacity per spin with respect to temperature for (a) 2D-$MnPX_3$, (b) Li:2D-$MnPX_3$, (c) Cl:2D-$MnPX_3$, (d) F:2D-$MnPX_3$.

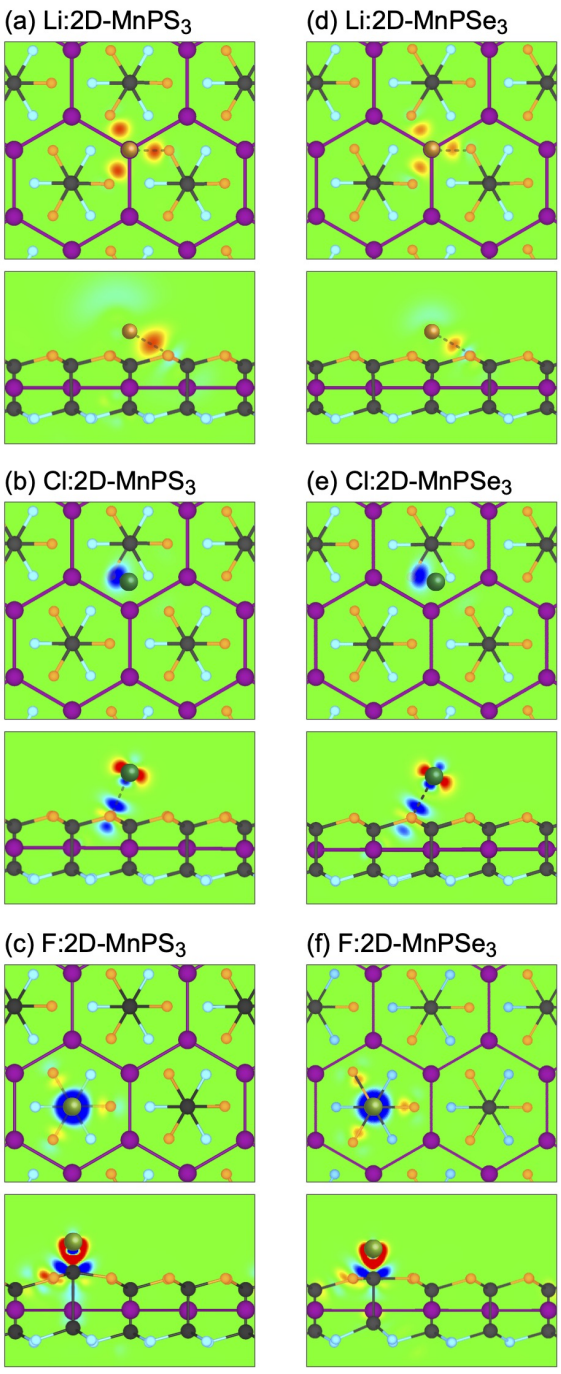

FIG. S7. Top and side views of the studied systems in their lowest energy configurations. Spheres of different size and colour represent atoms of different types (cf. Figure S1). The structures are overlaid with an electron charge difference maps $\Delta\rho(\mathbf{r}) = \rho_{\mathrm{sub/ads}}(\mathbf{r}) - [\rho_{\mathrm{sub}}(\mathbf{r}) + \rho_{\mathrm{ads}}(\mathbf{r})]$ (sub: substrate, ads: adsorbate). $\Delta\rho$ is colour coded as blue ($-0.01\,e/\mathrm{\AA}^3$), green (0), and red ($0.01\,e/\mathrm{\AA}^3$).

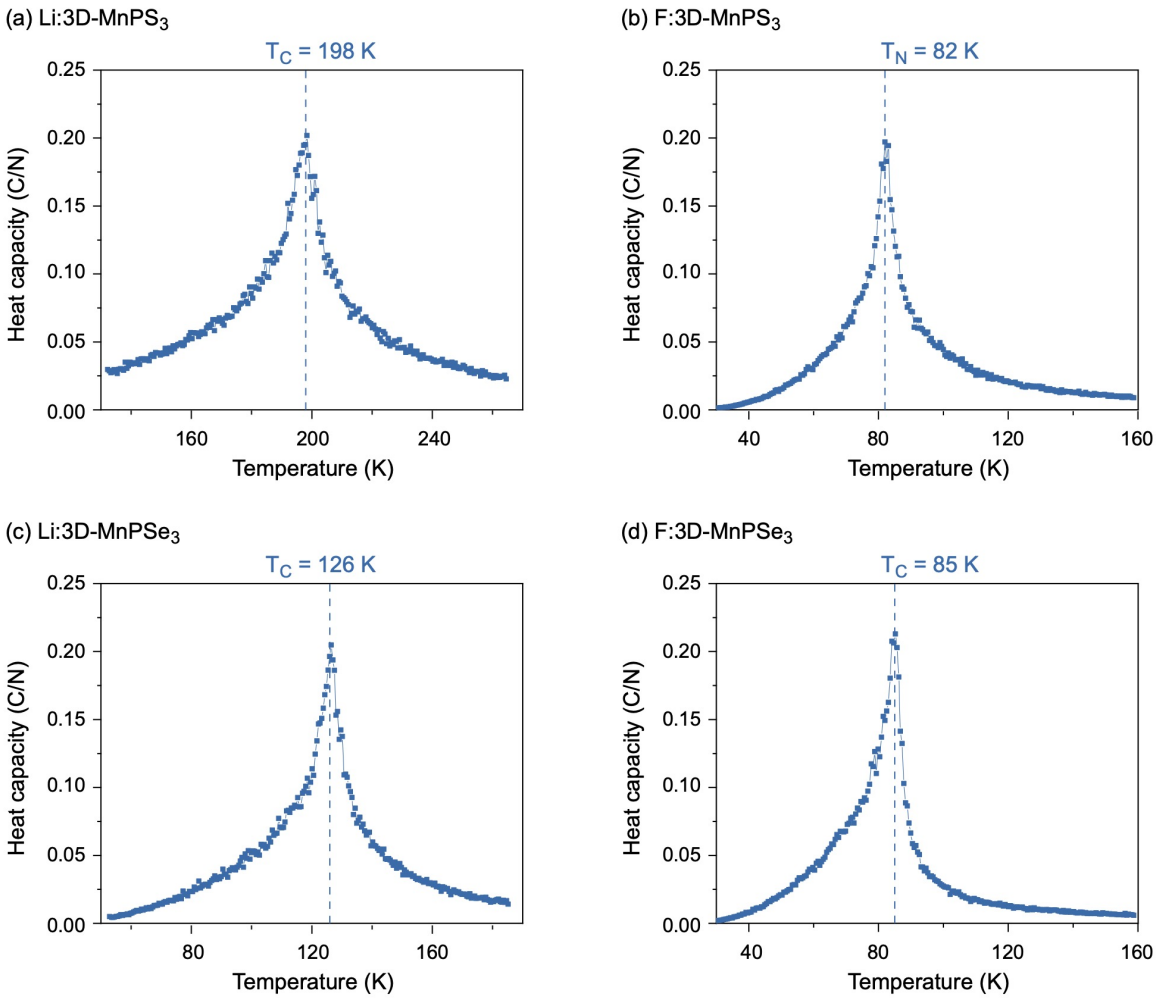

FIG. S8. Specific heat capacity per spin with respect to temperature for (a) Li:3D-$MnPS_3$, (b) F:3D-$MnPS_3$, (c) Li:3D-$MnPSe_3$, (d) F:3D-$MnPSe_3$.